ELSEVIER

Polymer 41 (2000) 4169–4177

polymer

Molecular simulation of gas solubilities in crystalline poly(α-alkyl-β-L-aspartate)s

D. Zanuy, S. León, C. Alemán*, S. Muñoz-Guerra

Departament d'Enginyeria Química, E.T.S. d'Enginyers Industrials de Barcelona, Universitat Politècnica de Catalunya, Diagonal 647, Barcelona E-08028, Spain

Received 29 March 1999; received in revised form 2 July 1999; accepted 2 September 1999

Abstract

We have studied the solubility of a small probe particle, the atoms He and Ar and the molecule CH_4 in the helical poly(α-alkyl-β-L-aspartate)s using molecular simulations. The hexagonal and tetragonal crystal forms of poly(α-*n*-butyl-β-L-aspartate) and the hexagonal form of the poly(α-methyl-β-L-aspartate) have been chosen for the study as the most representative structures for this family of polymers. An important characteristic of these structures is that the helical conformations are retained at high temperatures. The excess chemical potentials have been determined using Widom's test-particle insertion method considering an ensemble of microstructures generated by Monte Carlo calculations. The solubility of the different penetrants in the polymer systems was explained in terms of the distribution of the unoccupied space.

Keywords: Solubility; Molecular simulation; Poly(α-alkyl-β-L-aspartate)s

1. Introduction

The application of atomistic simulations to study the solubility of gas molecules in dense polymers has become a topic of broad interest in recent years due to the availability of more powerful computers [1,2]. These simulations are able to afford information about the polymer and/or the penetrant that is not readily accessible from experiments. Thus force-field simulations have provided a description of the mechanism of gas permeation in terms of the *free volume*. It should be mentioned that the term *free volume* in the context of gas transport refers to the volume not occupied by the atoms in the system [3,4]. Furthermore, atomistic simulations have confirmed that diffusion involves jumps of the gas molecules in the polymeric matrix, i.e. the hopping mechanism deduced 50 years ago [1,5–7]. In such a description the movement of the gas molecules is thought to be coupled to the elastic motion of the polymer chains but it is independent from the structural relaxation of the polymeric matrix.

Computational studies usually involve the solubility of gas molecules in amorphous host polymers. This is because the mobility of the penetrant is much higher in the amorphous phase than in the crystalline phase since the packing of the chains is much more loose in the former state. Accordingly, it has been traditionally accepted that the transport of gases in a semicrystalline polymer takes place mainly through the amorphous phase and so it has been confirmed in recent studies [8]. However, Puleo et al. [9] demonstrated that poly(4-methyl-1-pentene) (Fig. 1), abbreviated PMP displayed an exceptional behavior since similar permeabilities were found for the amorphous and crystalline regions. This finding is supported by the fact that the crystalline and amorphous densities in PMP are very similar and, therefore, the two phases should have a nearly equal amount of *free volume*. The crystal structure of PMP was determined by Tadokoro and coworkers [10]. It consists of four 7/2 helices packed together to form a tetragonal unit cell. In this structure the packing of the helices is very inefficient due to the presence of bulky and flexible pendent groups. The diffusion of carbon dioxide and methane in crystalline PMP was investigated at the atomistic level by Müller-Plathe using molecular dynamics simulations [11]. The results allowed to understand better the behavior of these penetrants in crystalline PMP and the unusually low barrier to gas diffusion displayed by this polymer.

Poly(α-alkyl-β-L-aspartate)s are nylon 3 derivatives with an alkoxycarbonyl group stereoregularly attached to every third backbone carbon atom of the repeating unit [12]. A schematic representation of the chemical formula of this

* Corresponding author. Tel.: +34-93401-6680/6681; fax: +34-93401-6600/7150.

E-mail address: aleman@eq.upc.es (C. Alemán).

0032-3861/00/$ - see front matter
PII: S0032-3861(99)00635-7

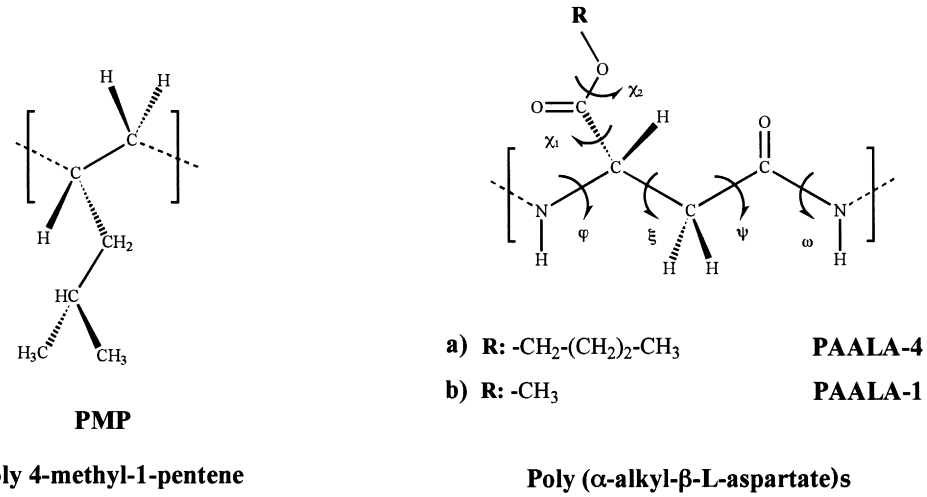

Fig. 1. Structure formulae of the repeating units of poly(4-methyl-1-pentene) and poly(α-alkyl-β-L-aspartate)s. Notations used for the dihedral angels in poly(α-alkyl-β-L-aspartate) are indicated.

family of polymers is given in Fig. 1. Recent studies on a number of poly(α-alkyl-β-L-aspartate)s including a variety of side chain compositions have shown that they adopt helical structures with features similar to those of the α-helix of polypeptides [13–19]. The most frequent helical arrangement found in the solid state for poly(α-alkyl-β-L-aspartate)s is the right-handed 13/4 helix, with intramolecular hydrogen bonds set between the amide groups i and $i + 3$. A second important conformation is the 4/1 helix based on an $i - i + 4$ hydrogen-bonding scheme. Other related helices occasionally observed are those consisting of 16/5 and 17/4 arrangements [15,16], which are closely related to the 13/4 helix and 4/1 helices, respectively.

The mode of packing and degree of ordering achieved in these systems are known to be largely dependent on the length of the alkyl side groups. Thus, the so-called hexagonal form, which is a monoclinic lattice of up-and-down chains in the $P2_1$ space group, is a structure invariably found in poly(α-alkyl-β-L-aspartate)s with alkyl side chains containing up to five carbon atoms [13–15]. In addition a second polymorph with a tetragonal structure in the space group $P4_1$ is observed when the polymer adopts the 4/1 helical conformation. On the other hand, a biphasic structure with 13/4 helices arranged in layers and side chains crystallized in a separated phase has been observed for derivatives bearing linear alkyl groups with 12, 18 and 22 carbon atoms [18,19]. An important characteristic of all these structures is that the backbone helical conformations are retained at high temperatures remaining immobilized in the crystal lattices, as revealed X-ray diffractograms recorded at different temperatures [18].

There are significant resemblances between the crystal structures of poly(α-alkyl-β-L-aspartate)s, in particular of those bearing short to medium size linear side chains, and that of PMP: (i) their molecular chains adopt helical conformations with a relatively close symmetry; (ii) the 4/1 helices of poly(α-alkyl-β-L-aspartate)s pack in a tetragonal lattice similar to that found for the 7/2 helices of PMP; and (iii) the flexible side groups protrude from the main chain to invade the intermolecular space in a similar manner. Furthermore, it should be noticed that poly(α-alkyl-β-L-aspartate)s present a lower density of side groups than PMP so that a larger *free volume* should be expected a priori for the formers. Accordingly, a study about the behavior of small penetrants in poly(α-alkyl-β-L-aspartate)s is highly desirable.

In this work we present a predictive study about the behavior of small gas molecules in some crystalline poly(β-L-aspartate)s using molecular simulations. Since no experimental evaluation is available at the present time, simple penetrants He, Ar and CH_4 were chosen. In addition a probe particle (abbreviated SPP) with a size even smaller was analyzed. The systems investigated were the hexagonal and tetragonal forms of poly(α-*n*-butyl-β-L-aspartate) (PAALA-4) and the hexagonal form of poly(α-methyl-β-L-aspartate) (PAALA-1), which are the most representative crystal structures of this family of polymers. To generate a number of PAALA-4 and PAALA-1 microstructures, we performed Monte Carlo calculations in periodic simulation cells where the conformation of the side chains were allowed to vary. The excess chemical potentials were then computed using an efficient implementation of Widom's test-particle insertion method [20].

2. Methods

2.1. Starting structures

The starting geometries for the different structures investigated were taken from our previous works [14,15]. The unit cell for the hexagonal and tetragonal forms of PAALA-4 are ($a = 13.4$ Å, $c = 20.60$ Å) and ($a = 14.1$ Å, $c = 4.90$ Å), respectively, whereas the unit cell of the hexagonal form of PAALA-1 is ($a = 12.03$ Å, $c = 20.51$ Å). The

Table 1
Crystallographic parameters and dihedral angles (in °) for the helical conformations of PAALA-4 and PAALA-1 obtained from the refinements against the X-ray data

Polymer	Helix	Crystal form	Unit cell (Å)	Space group	ϕ	ξ	ψ	ω	χ_1	χ_2	χ_i $(i = 2,5)$
PAALA-4	13/4	Hexagonal	$a = 13.4$; $c = 20.60$	$P2_1$	146.2	−59.8	128.8	180.0	173.4	180.0	180.0
PAALA-4	4/1	Tetragonal	$a = 14.1$; $c = 4.90$	$P4_1$	144.4	−87.2	148.1	180.0	146.4	180.0	180.0
PAALA-1	17/4	Hexagonal	$a = 12.03$; $c = 20.51$	$P2_1$	141.7	−92.3	155.4	180.0	145.8	180.0	–

position of the helices within the unit cell as well as the conformational parameters of the three types of helices were refined against the X-ray diffraction data in previous works [14,15]. Table 1 reports the crystallographic parameters and dihedral angles obtained from these refinements for the 13/4 and 4/1 helices of PAALA-4 and the 17/4 helix of PAALA-1. The projection along the *c*-axis of the three crystal forms investigated is displayed in Fig. 2.

2.2. Generation of microstructures

A number of microstructures for the hexagonal and tetragonal forms of PAALA-4 and the hexagonal form of PAALA-1 was required in order to study the solubility of the penetrants in these systems. They were obtained using an advanced Monte Carlo sampling technique (continuum configurational bias, CCBMC), which has already been found to be efficient in the study of dense systems [21,22]. In addition to CCB moves, a small fraction (20%) of Metropolis moves were also used. It should be remarked that the generated microstructures only differ in the conformations of the flexible side chains and that the helices within the unit cell were retained in the positions observed by X-ray diffraction (see later). The simulations started from the unit cells described in Section 2.1 and showed in Fig. 3. The boxes used in the simulation consist of four independent chains of 13, 12 and 17 residues for the hexagonal and tetragonal forms of PAALA-4 and the hexagonal form of PAALA-1, respectively. The size and density of the boxes used for the simulations are displayed in Table 2, where the experimental density is also included for comparison. Periodic continuation conditions and the minimum-image convention were applied to all simulations. MC simulations of 100,000 steps of the NVT type, i.e. without varying the size of the cell, were performed at 298 K after equilibration. For each simulation 50 microstructures were sampled at 2000 steps intervals.

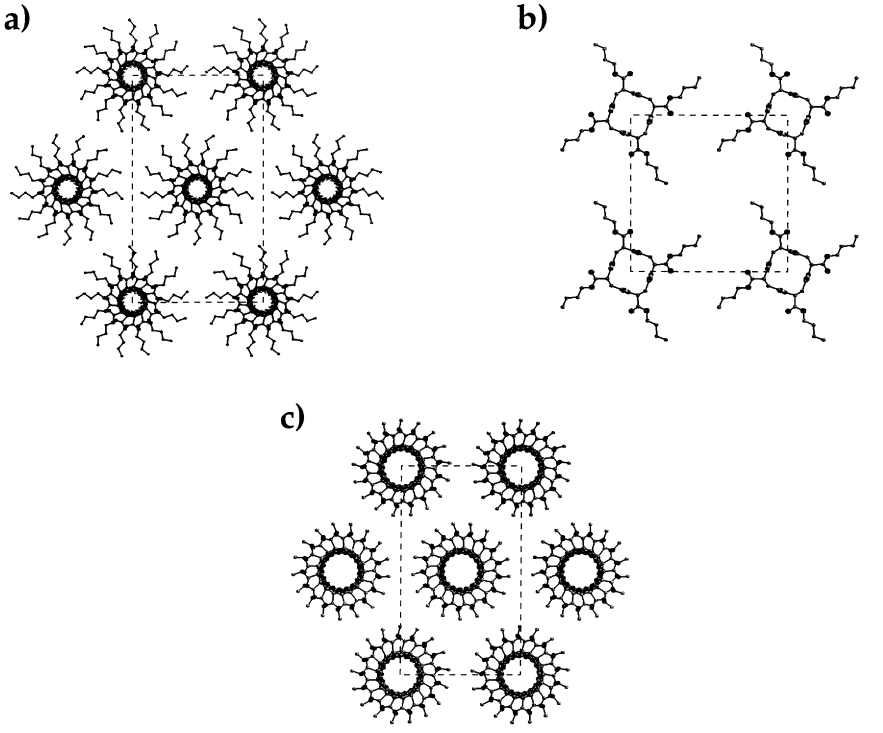

Fig. 2. Projection along the *c*-axis of the unit cells of the: (a) hexagonal form of poly(α-*n*-butyl-β-L-aspartate) 13/4 helices; (b) tetragonal form of poly(α-*n*-butyl-β-L-aspartate) 4/1 helices; and (c) hexagonal form of poly(α-methyl-β-L-aspartate) 17/4 helices. The chains have been drawn with an increased separation between them in order to show the molecular arrangement more clearly.

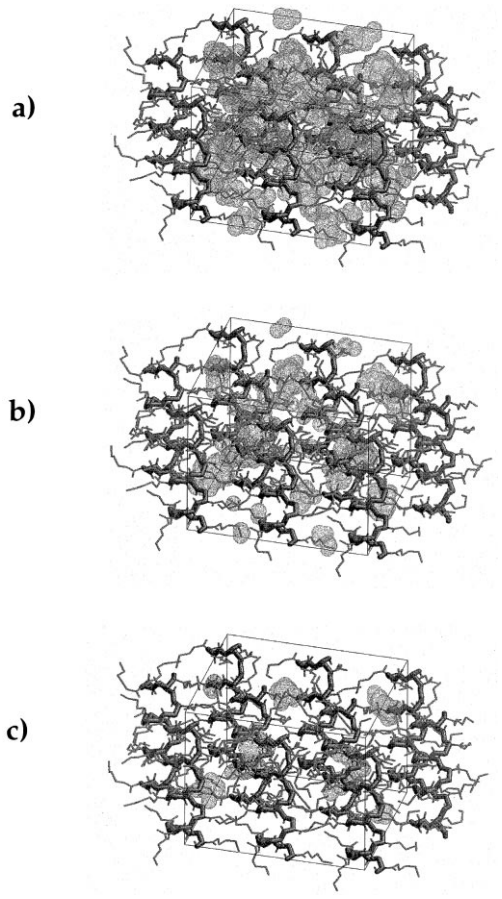

Fig. 3. Unoccupied space for (a) SPP, (b) He (c) and Ar penetrants in one of the microstructures generated for the hexagonal form of poly(α-*n*-butyl-β-L-aspartate).

The model used in the MC calculations assumed fixed bond lengths and bond angles for the side chains; main chain dihedral angles were entirely fixed to the values found from the refinement of the X-ray data (see Table 1). The assumption of fixed backbones is quite reasonable for the systems under study since X-ray diffraction studies at different temperatures clearly revealed that the corresponding helical conformations are retained at high temperatures [18]. Helix centers, defined as the intersections of helix axes (running along the *z*-direction) with *xy*-plane, were fixed relative to the unit cell, i.e. they remained fixed during all the moves. The only degrees of freedom of the system were therefore the torsional angles associated to the ethylene bonds of the side chains. The AMBER [23] force field was used to represent the van der Waals and torsional energies of the system. Electrostatic interactions were neglected since all the polar groups were kept fixed along the simulations. The results of preliminary calculations using models of all atoms and united atoms models for both methyl and methylene groups were very similar. Accordingly, the model of united atoms was used due to its lower computational cost. The van der Waals energy was computed in the usual pairwise additive way using a Lennard-Jones 6–12 potential. Lennard-Jones potentials were truncated at 8 Å.

Table 2
Size (in Å) and density (ρ, in g/ml) of the boxes used for the Monte Carlo simulations (experimental densities (ρ_{exp}) are also displayed for comparison)

PAALA	Crystal form	*a*	*b*	*c*	ρ	ρ_{exp}
PAALA-4	Hexagonal	26.9	23.3	20.60	1.18	1.17
PAALA-4	Tetragonal	28.2	28.2	14.73	1.21	1.18
PAALA-1	Hexagonal	24.06	20.89	21.90	1.33	1.36

Table 3
Lennard-Jones potential parameters for the penetrants

Penetrant	*R* (Å)	ϵ (kcal/mol)
SSP	0.93	0.010
He	1.30	0.020
Ar	1.70	0.238
CH_4	1.91	0.294

2.3. Free volume measurements

The unoccupied space in a given microstructure was estimated using the van der Waals radii of both the penetrant and polymer. This was done by dividing the simulation box of every microstructure into a three-dimensional uniformly spaced grid. These grids consisted of 975529, 893101 and 794325 nodes for the hexagonal and tetragonal forms of PAALA-4 and the hexagonal form of PAALA-1, respectively. Then, a penetrant was centered in each node and the distance to the nearest atom of the polymeric matrix was measured. If this distance was larger than the sum of the van der Waals radii of the penetrant and the polymer atom the node was identified as unoccupied. The van der Waals radii used for the penetrants are displayed in Table 3, whereas those of the polymer atoms were taken from the AMBER libraries [23].

2.4. Widom's test-particle insertion method

The infinite-dilution excess chemical potentials of a penetrant sorbed in poly(β-L-aspartate)s structures were estimated using Widom's test-particle insertion method [24,25]. In this method the chemical potential of species *i* in a frozen *N*-particle system relative to an ideal gas mixture is related to the potential energy of inserting a test-particle into the system at randomly chosen positions. The expression for the excess chemical potential is:

$$\beta\mu_i^{ex}(\rho,T) = -\ln\langle\exp(-\beta\phi_t)\rangle_N \quad (1)$$

where $\beta = 1/k_BT$, ϕ_t is the interaction energy between the test-particle and the *N* particles of the system, and $\mu_i^{ex}(\rho,T)$ is the excess of chemical potential of species *i* at temperature *T* and number density $\rho = N/V$. The brackets $\langle\cdots\rangle_N$

Table 4
Fraction of predicted *free volume* (averaged over the 50 microstructures generated by MC simulations) (V_{free}; in %) for the different penetrants (the V_{free} for CH_4 was zero in all the cases) in the hexagonal and tetragonal forms of PAALA-4 and the hexagonal form of PAALA-1 [the standard deviation (σ; in %) and the maximum and minimum values (in %) of the *free volume* for each set of microstructures are also displayed]

Polymer	Form	Diffusant	V_{free}	σ	Maximum	Minimum
PAALA-4	Hexagonal	SPP	6.24	±0.35	7.05	5.49
		He	2.37	±0.27	3.02	1.89
		Ar	0.70	±0.16	1.09	0.41
PAALA-4	Tetragonal	SPP	2.70	±0.21	3.08	2.13
		He	0.62	±0.15	0.94	0.31
		Ar	0.08	0.03	0.16	0.01
PAALA-1	Hexagonal	SPP	2.95	±0.04	3.04	2.87
		He	0.26	±0.02	0.29	0.23
		Ar	< 0.01	–	–	–

denote the canonical ensemble average over the original N-particle system (without test-particle) at the T and ρ of interest. The test-particle insertion method has been used successfully at low to moderate fluid densities [26–28]. However, at high densities the method becomes inefficient as it becomes increasingly unlike that a test particle can be inserted successfully into the fluid. That is, the insertions that provide a positive value for ϕ_t due to repulsive overlaps in a high-density fluid have a negligible contribution to μ_i^{ex} (see Eq. (1)). Different methods have been proposed to obtain significant improvements in the insertion efficiency [20,28–33]. These studies have revealed that a satisfactory approximation is achieved by searching only those regions where successful particle insertions are more likely to occur [20,31–33]. Within this framework Cuthbert et al. [20] defined the ensemble average $\langle \exp(-\beta\phi_t)\rangle_N$ (Eq. (1)) as follows:

$$\langle \exp(-\beta\phi_t)\rangle_N = \sum_{j=1}^{N_e} (1/N_{T,j}) \sum_{i=1}^{N_{V,j}} \exp(-\beta\phi_{t,i}) \quad (2)$$

where $N_{V,j}$ is the number of sites without overlaps in the microstructure j, $N_{T,j}$ is the total number of insertions for a given microstructure j assuming a uniform insertion density, and N_e is the total number of microstructures available for computing the ensemble of averages.

We have used Eq. (2) to compute the excess chemical potential. For this purpose, we have divided the microstructures into uniformly spaced grids. A penetrant particle was centered in each node only if it is identified as unoccupied. Calculations were performed considering spacings between consecutive nodes of 1, 0.75, 0.50 and 0.25 Å. In order to normalize this biased sampling, the average of μ_i^{ex} for each microstructure was weighted by $\omega_j = N_{V,j}/N_{T,j}$ before being summed to yield the ensemble average. Lennard-Jones interactions between the penetrants and the polymer atoms were computed using a Lennard-Jones 6–12 potential and applying the standard Lorentz–Berthelot mixing rules. The force-field parameters used for the penetrants are displayed in Table 3. The interaction energies were truncated at 8 Å.

3. Results and discussion

In order to ensure that the generated microstructures are statistically independent we computed for the three systems under study the first and second degree bond autocorrelation functions as well as the relaxation function of the end-to-end distance vector [34]. All these functions decay rapidly to small values (data not shown) following the same behavior predicted for polyethylene chains [34]. These results indicate that the microstructures recorded out of each other by 2000 MC moves are independent.

As a first step of MC data evaluation, we examined the unoccupied space of all the generated microstructures. These results are summarized for each penetrant in Table 4, which displays the amount of *free volume* averaged over the 50 microstructures recorded for the three systems under study. It is worth to note that for PAALA-4 the largest *free volume* results for the hexagonal form, being about two times that of the tetragonal form for all the penetrants. This correlates well with the measured densities, which are 1.06 and 1.18 g/ml, respectively. On the other hand, the amount of *free volume* predicted for the hexagonal form of PAALA-1 is close to that of tetragonal form of PAALA-4. The large density measured for the hexagonal form of PAALA-1 (1.36 g/ml) revealed that it has a much more compact structure than the hexagonal form of PAALA-4. This is in part due to the different hydrogen bonding scheme adopted by these two polymers. In fact the central hole of the 17/4 helix of PAALA-1 is wider than that of the 13/4 helix of PAALA-4 (Fig. 2) providing the former with a more compact crystal packing of the side chains.

As can be seen from the small standard deviations of the averages as well from both the maximum and minimum values of the predicted *free volume* within each set of microstructures (see Table 4), all the models generated for a given polymer present a similar unoccupied space. This trend suggests that the number of microstructures generated is suitable for the present study.

An analysis of the results obtained for the different penetrants reveals some important features. As can be expected,

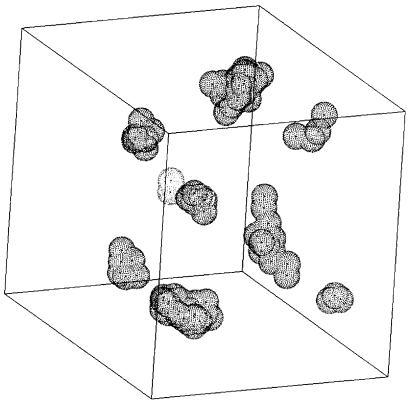

Fig. 4. Ellipsoid-shaped cavities for Ar penetrant in one of the microstructures generated for the hexagonal form of PAALA-4.

the *free volume* decreases when the size of the penetrant increases, being zero in all the cases for CH_4. These results further indicate that a number of SPP, He and Ar molecules are able to fit within the hexagonal form of PAALA-4, whereas the space available for the latter penetrant in the tetragonal form of PAALA-4 and the hexagonal form of PAALA-1 is very small. Thus, the ratios that relate the *free volume* for the different penetrants drastically increase with the density of the system. Thus, in the hexagonal form of PAALA-4 the *free volume* for SPP is a factor of 2.6 and 8.9 larger than those for He and Ar, respectively. These factors increase to 4.5 and 33.7 for the tetragonal form of PAALA-4, and to 11.3 and >100 for the hexagonal form of PAALA-1.

A visual inspection of the volume accessible to the penetrants in microstructures of the hexagonal form of

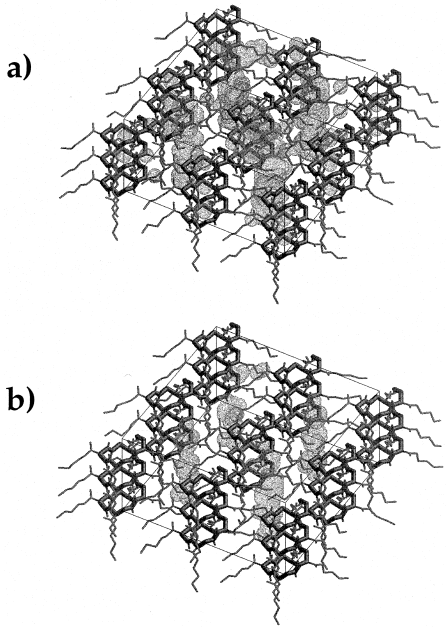

Fig. 5. Unoccupied space for (a) SPP (b) and He penetrants in one of the microstructures generated for the tetragonal form of poly(α-*n*-butyl-β-L-aspartate).

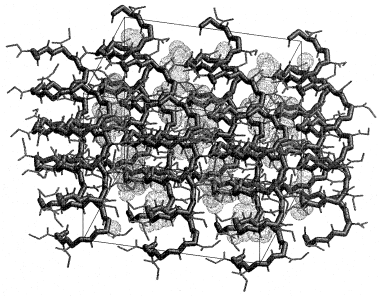

Fig. 6. Unoccupied space for SPP penetrant in one of the microstructures generated for the hexagonal form of poly(α-methyl-β-L-aspartate).

PAALA-4 reveals their cavernous distribution. Fig. 3 depicts the *free volume* for SPP, He and Ar in one of the microstructures. Typically, the cavities are ellipsoids with 3–9, 3–7 and 3–6 Å in length for SPP, He, and Ar, respectively. Fig. 4 shows a detailed view of the ellipsoid-shaped cavities for Ar in one of the microstructures. In all cases these ellipsoids are less than 3.5 Å in width. For the SPP penetrant, the cavities are occasionally separated by a bottleneck of about 3–4 Å in length and 1–2 Å in width allowing the easy passage from one cavity to other. On the other hand, we never found long channels constituted by a number of cavities connected by passages.

Analysis of the *free volume* for the SPP and He penetrants in microstructures of the tetragonal form of PAALA-4 revealed a completely different distribution of the unoccupied space. Thus, about 70 and 16% of the microstructures display one or more channels crossing the simulation box for SPP and He, respectively. Fig. 5 illustrates the presence of channels for SSP and He in one microstructure. These channels are about 1.5–3.5 and 1.5–2.25 Å in width, respectively. This is a surprising result since the *free volume* is smaller for the tetragonal form than for the hexagonal form. This apparently anomalous behavior is due to the more ordered packing of the side chains in the former form. On the contrary, a cavernous distribution of the accessible volume similar to that of the hexagonal form was detected when Ar was the tested penetrant.

A cavernous distribution of the *free volume* was also found for the hexagonal form of PAALA-1. The cavities are 3–5 and 2–3 Å in size for SPP and He penetrants, respectively. Bottlenecks of about 2 Å in length and 1.5 Å in width connecting different cavities were found for SSP, whereas no passage was found for He. As was discussed before no cavity was found for Ar. Fig. 6 shows the distribution of the *free volume* for SSP in one of the microstructures of PAALA-1 with no channels outlined.

Table 5 shows the calculated excess chemical potentials for the three structures investigated considering grid spacings of 1, 0.75, 0.50 and 0.25 Å. The results indicate that grid spacings finer than 0.75 Å displayed no significant changes in the resulting excess chemical potential of the hexagonal and tetragonal forms of PAALA-4. Conversely, the excess chemical potential for PAALA-1 fluctuates when

Table 5
Excess chemical potentials (kcal/mol) for the different penetrants in the hexagonal and tetragonal forms of PAALA-4 and the hexagonal form of PAALA-1

Penetrant	Grid spacing	PAALA-4 Hex	PAALA-4 Tet	PAALA-1 Hex
SPP	1	−2.17	−1.66	1.73
	0.75	−2.18	−1.68	−1.72
	0.50	−2.18	−1.68	−1.69
	0.25	−2.19	−1.68	−1.65
He	1	−1.60	−0.81	−0.29
	0.75	−1.62	−0.80	−0.18
	0.50	−1.62	−0.82	−0.26
	0.25	−1.63	−0.83	−0.23
Ar	1	−0.81	0.38	–
	0.75	−0.91	0.34	–
	0.50	−0.91	0.37	–
	0.25	−0.93	0.37	–

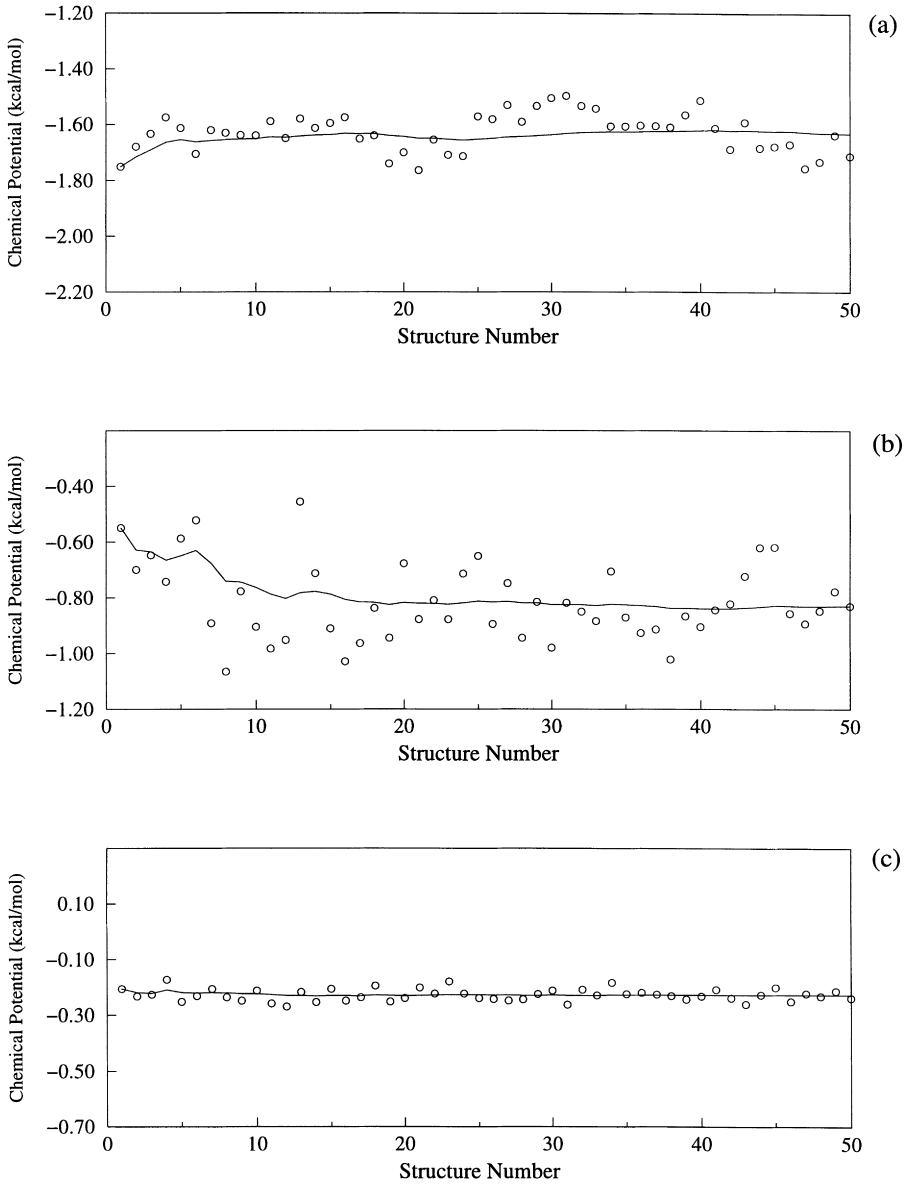

Fig. 7. Convergence of the excess chemical potential of He calculated using Widom's test-particle insertion method in the 50 microstructures obtained from MC calculations for the: (a) hexagonal form of poly(α-*n*-butyl-β-L-aspartate); (b) tetragonal form of poly(α-*n*-butyl-β-L-aspartate); and (c) hexagonal form of poly(α-*n*-methyl-β-L-aspartate).

the size of the grid changes. This could be due either to using an insufficient number of microstructures to converge the process or to the particular distribution of the *free volume* in this polymer. Fig. 7 shows the progress of the excess chemical potential of He for the 50 generated microstructures of the three polymers considering a grid spacing of 0.25 Å. Each point corresponds to one application of Eq. (1) to one of the 50 microstructures generated from MC simulations whereas the solid line displays the mean value of resulting excess chemical potential up to this microstructure. It is worth to note that the line drawn is running average over the points indicating the convergence of these calculations. Accordingly, we can conclude that the fluctuating behavior of the resulting excess chemical potential for PAALA-1 is due to the cavernous distribution of the *free volume* in this system. Thus, it should be emphasized that although the hexagonal form of PAALA-4 also presents a similar distribution of the *free volume*, the size of the cavities is considerably higher due to its lower density (see Table 4).

The results displayed in Table 5 indicate that the interactions of both SPP and He penetrants with the polymer matrix are favorable in all cases. Within a given crystal form the strength of these interactions decreases with the size of the penetrant, whereas for a given penetrant the interactions are more favorable when the amount of *free volume* increases. It is seen as Ar has a significantly higher excess chemical potential in the tetragonal form of PAALA-4 relative to the hexagonal form. These less favorable interactions would result from a larger number of low-energy configurations when Ar is inserted into the polymer matrix. Thus, the small amount of *free volume* for Ar indicates that there are few cavities inside the polymer matrix that are of sufficient size to stabilize the insertion of this penetrant.

Results achieved in this study indicate that the solubility of small penetrants in poly(α-alkyl-β-L-aspartate)s is lower than that observed and predicted for crystalline PMP [9,11] as a logical consequence of the smaller amount of *free volume* present in those polymers. Furthermore, the *free volume* in PMP is distributed in channels of sufficient size to accommodate CO_2 and CH_4 gas molecules. Conversely, the hexagonal forms of PAALA-1 and PAALA-4 present an irregular distribution of the *free volume*. On the other hand, the unoccupied space of tetragonal form of PAALA-4 is distributed in channels, although they continue to be unable to fit penetrants higher than He.

4. Conclusions

We have performed a molecular simulation study of the solubility of small gaseous penetrants in crystalline poly(α-alkyl-β-L-aspartate)s. More specifically, the solubilities of SPP, He, Ar and CH_4 in the hexagonal and tetragonal forms of PAALA-4 and the hexagonal form of PAALA-1 were predicted using Widoms test-particle insertion method. A number of microstructures were generated for the three crystal forms using an advanced Monte Carlo sampling technique.

A cavernous distribution of the *free volume* was found for the hexagonal form of PAALA-4 and PAALA-1, the dimensions of the cavities precluding the accommodation of penetrants larger than Ar and He, respectively. On the other hand, a number of microstructures with channels were detected for the tetragonal form of PAALA-4. The size of the channels was sufficient to accommodate SPP and He particles but not Ar. In all the systems investigated the holes were too small to permit the solubility of CH_4. The calculated excess chemical potentials reveal favorable interactions between the polymer matrix and the two smallest penetrants SPP and He, for the three crystal forms. However, Ar was predicted to be soluble in the hexagonal form of PAALA-4 but not in the tetragonal form. The large excess chemical potential predicted for this gas in the tetragonal form of PAALA-4 was caused by the much stronger repulsive Lennard-Jones interactions. The present results indicate that small gaseous penetrants present a lower solubility in poly(α-alkyl-β-L-aspartate)s than crystalline PMP even though both types of compounds share many structural features.

Acknowledgements

This work was supported by DGICYT with grant no. PB96-0490. D.Z. and S.L. acknowledge the support of the Ministry of Education of Spain for the award of a scholarship. Authors wish to thank Prof M. Laso, Universidad Politécnica de Madrid, for assistance in the preparation of MC simulations.

References

[1] Gusev AA, Müller-Plathe F, van Gunsteren WF, Suter UW. Adv Polym Sci 1994;116 p. 116, 207.
[2] Müller-Plathe F. Acta Polym 1994;45:259.
[3] Arizzi S, Mott PH, Suter UW. J Polym Sci Part B 1992;30:415.
[4] Vrentas JS, Duda JL. J Polym Sci, Polym Phys Ed 1977;15:403.
[5] Sok RM, Berendsen HJC, van Gunsteren WF. J Chem Phys 1992;96:4699.
[6] Müller-Plathe F. J Chem Phys 1991;94:3192.
[7] Sonnenburg J, Gao J, Weiner JH. Macromolecules 1990;23:4653.
[8] Müller-Plate F. Chem Phys Lett 1991;177:527.
[9] Puleo AC, Paul DR, Wong PK. Polymer 1989;30:1357.
[10] Kusanagi H, Takase M, Chatani Y, Tadokoro H. J Polym Sci, Polym Phys Ed 1978;16:131.
[11] Müller-Plathe F. J Chem Phys 1995;103:4346.
[12] Fernández-Santín JM, Aymamí J, Rodríguez-Galán A, Muñoz-Guerra S, Subirana JA. Nature (London) 1984;311:53.
[13] López-Carrasquero F, Alemán C, García-Alvarez M, Martínez de Ilarduya A, Muñoz-Guerra S. Makromol Chem Phys 1995;196:253.
[14] Navas JJ, Alemán C, López-Carrasquero F, Muñoz-Guerra S. Macromolecules 1995;28:4487.
[15] López-Carrasquero F, García-Alvarez M, Navas JJ, Alemán C, Muñoz-Guerra S. Macromolecules 1996;29:8449.

[16] García-Alvarez M, León S, Alemán C, Campos JL, Muñoz-Guerra S. Macromolecules 1998;32:124.
[17] García-Alvarez M, Martínez de Ilarduya A, León S, Alemán C, Muñoz-Guerra S. J Phys Chem A 1997;101:4215.
[18] López-Carrasquero F, Montserrat S, Martínez de Ilarduya A, Muñoz-Guerra S. Macromolecules 1995;28:5535.
[19] Navas JJ, Alemán C, López-Carrasquero F, Muñoz-Guerra S. Polymer 1997;38:3477.
[20] Cuthbert TR, Wagner NJ, Paulaitis ME. Macromolecules 1997;30:3058.
[21] de Pablo JJ, Laso M, Suter UW. J Chem Phys 1992;96:6157.
[22] de Pablo JJ, Laso M, Suter UW. Macromolecules 1993;26:6180.
[23] Weiner SJ, Kollman PA, Case DA, Singh UC, Ghio C, Alagona G, Profeta S, Weiner P. J Am Chem Soc 1984;106:765.
[24] Widom B. J Phys Chem 1982;86:869.
[25] Widom B. J Chem Phys 1963;39:2808.
[26] van der Vegt NFA, Briels WJ, Wessling M, Strathmann H. J Chem Phys 1996;105:8849.
[27] Bicerano J, Moll DJ. Comput Polym Sci 1996;6:117.
[28] Torrie GM, Valleau JP. Chem Phys Lett 1974;28:578.
[29] Knopp B, Suter UW, Gusev AA. Macromolecules 1997;30:6107.
[30] Knopp B, Suter UW. Macromolecules 1997;30:6114.
[31] Dietrick GL, Scriven LE, Davis HT. J Chem Phys 1989;90:2370.
[32] Sok RM, Berendsen HJC, van Gunsteren WF. J Chem Phys 1992;96:4699.
[33] Tamai Y, Tanaka H, Nakanishi K. Macromolecules 1995;28:2544.
[34] Leontidis E, de Pablo JJ, Suter UW. Adv Polym Sci 1994;116:283.